Stability of proICA512/IA-2 and Its Targeting to Insulin Secretory Granules Require β4-Sheet-Mediated Dimerization of Its Ectodomain in the Endoplasmic Reticulum

Juha M. Torkko,[a,b] M. Evangelina Primo,[c,d*] Ronald Dirkx,[a,b] Anne Friedrich,[a,b] Antje Viehrig,[a,b] Elisa Vergari,[a,b] Barbara Borgonovo,[a,f] Anke Sönmez,[a,b] Carolin Wegbrod,[a,b] Martina Lachnit,[a,b] Carla Münster,[a,b] Mauricio P. Sica,[d,e*] Mario R. Ermácora,[d,e] Michele Solimena[a,b,f]

Paul Langerhans Institute Dresden, Uniklinikum Carl Gustav Carus, TU Dresden, Germany[a]; German Center for Diabetes Research (DZD e.V.), Neuherberg, Germany[b]; University of Buenos Aires, Buenos Aires, Argentina[c]; Instituto Multidisciplinario de Biología Celular, Consejo Nacional de Investigaciones Científicas y Técnicas, Buenos Aires, Argentina[d]; Departamento de Ciencia y Tecnología, Universidad Nacional de Quilmes, Bernal, Buenos Aires, Argentina[e]; Max Planck Institute of Molecular Cell Biology and Genetics, Dresden, Germany[f]

The type 1 diabetes autoantigen ICA512/IA-2/RPTPN is a receptor protein tyrosine phosphatase of the insulin secretory granules (SGs) which regulates the size of granule stores, possibly via cleavage/signaling of its cytosolic tail. The role of its extracellular region remains unknown. Structural studies indicated that β2- or β4-strands in the mature ectodomain (ME ICA512) form dimers *in vitro*. Here we show that ME ICA512 prompts proICA512 dimerization in the endoplasmic reticulum. Perturbation of ME ICA512 β2-strand N-glycosylation upon S508A replacement allows for proICA512 dimerization, *O*-glycosylation, targeting to granules, and conversion, which are instead precluded upon G553D replacement in the ME ICA512 β4-strand. S508A/G553D and N506A/G553D double mutants dimerize but remain in the endoplasmic reticulum. Removal of the N-terminal fragment (ICA512-NTF) preceding ME ICA512 allows an ICA512-ΔNTF G553D mutant to exit the endoplasmic reticulum, and ICA512-ΔNTF is constitutively delivered to the cell surface. The signal for SG sorting is located within the NTF RESP18 homology domain (RESP18-HD), whereas soluble NTF is retained in the endoplasmic reticulum. Hence, we propose that the ME ICA512 β2-strand fosters proICA512 dimerization until NTF prevents N506 glycosylation. Removal of this constraint allows for proICA512 β4-strand-induced dimerization, exit from the endoplasmic reticulum, *O*-glycosylation, and RESP18-HD-mediated targeting to granules.

Receptor protein tyrosine phosphatases (RPTPs) form a large family of transmembrane proteins which counteract protein tyrosine kinases and are therefore involved in many signaling pathways. Dimerization of RPTPs is regarded as a main mechanism to regulate their constitutive intracellular phosphatase activity. The contributions of extracellular, transmembrane, and cytoplasmic PTP regions to dimerization vary among different RPTPs (1–4).

The extracellular domains of RPTPs can promote receptor dimerization in several ways. As for receptor protein tyrosine kinases, RPTP oligomerization and clustering can be induced upon heterophilic binding to extracellular ligands. RPTPs for which such a mechanism has been demonstrated include the type I RPTP CD45/RPTPC, the type IIa protein RPTPσ, the type III protein RPTPβ, and the type V protein RPTPζ (5). In the case of CD45 and RPTPβ, changes in glycosylation pattern, including *O*-glycosylation, were shown to modulate their binding to galectin-1, conceivably increasing clustering and affecting phosphatase activity (6, 7). Homophilic interactions among ectodomains of RPTPs in the same or apposing cells, as is the case for the type IIb proteins RPTPμ and RPTPκ and the type IV protein RPTPα, likely represent another mechanism for inducing receptor oligomerization and regulating phosphatase activity (8–10).

The type VII RPTP ICA512/IA-2/PTPRN and its homologue phogrin/IA-2β/PTPRN2 are "pseudophosphatases" with a large ectodomain followed by a transmembrane region and a single catalytically inactive PTP domain (11, 12). They are expressed mainly in neuropeptidergic neurons and peptide-secreting endo-crine cells, including insulin-producing pancreatic β-cells, where they are enriched in secretory granules (SGs) (13, 14). Upon expression in *Escherichia coli*, the transmembrane regions of phogrin and ICA512 showed only weak or no ability to interact (2). On the other hand, in transfected fibroblasts, the cytosolic juxtamembrane and PTP domains of ICA512 and phogrin were shown to form homodimers as well as heterodimers with each other and with the PTP domains of other conventional RPTPs, possibly inhibiting their phosphatase activity (15). In insulinoma cells, homodimerization of the ICA512 PTP domain was found to disrupt the interaction of the latter with the cortical actin cytoskeleton, thereby affecting insulin SG dynamics and exocytosis (16).

Recent structural studies of the recombinant membrane-proximal mature ectodomain of ICA512 (ME ICA512/IA-2), which results from cleavage of proICA512 by prohormone convertases during SG maturation (13, 17), showed that this region readily adopted various dimeric assemblies both in the protein crystals and in solution (18, 19). In contrast, the corresponding recombinant mature ectodomain of phogrin, despite its structural similarity to ICA512 (20, 21), was found to fold as a monomer in solution (20, 21). In this study, therefore, we investigated the ability of ME ICA512 to induce receptor homodimerization in insulin-producing cells.

MATERIALS AND METHODS

Generation of ICA512 constructs and site-directed mutagenesis. pEGFP-N1 constructs encoding full-length human ICA512 (amino acids 1 to 979), an ICA512 N-terminal fragment (NTF) (amino acids 35 to 446), ICA512 ΔNTF (amino acids 449 to 979), the ICA512 regulated endocrine-specific protein 18 homology domain (RESP18-HD) (amino acids 35 to 131), or ME ICA512 (amino acids 449 to 575) were fused at their C termini to green fluorescent protein (GFP) or a hemagglutinin (HA) epitope tag. These constructs included either the native signal peptide or that of CD33, while an 11-mer linker was placed between ME ICA512 and GFP. Conventional cloning strategies were also used to generate ICA512-NTF or a secretory GFP by inclusion of the CD33 signal peptide at the N terminus. Site-directed mutagenesis using these constructs as templates was performed with a QuikChange kit (Stratagene). All constructs and mutations were verified by sequencing.

Antibodies against ICA512-NTF, ME ICA512, and ICA512 CT. Mouse monoclonal antibodies directed against a recombinant fusion protein between glutathione S-transferase (GST) and amino acids 389 to 575 (anti-ectodomain) or amino acids 935 to 974 (anti-ICA512 cytoplasmic tail [CT]) of human ICA512 were generated in the Antibody Facility at the Max Planck Institute of Molecular Cell Biology and Genetics (MPI-CBG; Dresden, Germany). The ectodomain antibodies were further selected for recognition of an epitope within amino acids 389 to 446 of the NTF (anti-ICA512 NTF Ab) or amino acids 449 to 575 of ME ICA512 (anti-ME ICA512 Ab) by using a MesoScale Discovery platform and by Western blotting against ICA512-NTF-GFP, ICA512-GFP ΔNTF, and GST.

Culture and transfection of insulinoma INS-1 cells. Rat INS-1 cells were grown in RPMI 1640 medium as described previously (22). Cells were split every 4 days, plated onto coverslips on 35-mm dishes (Costar), and transfected for 3 days, after with plasmid DNA was diluted into Cytoporation medium by use of a Cyto Pulse electroporator (Cyto Pulse Sciences, Inc.). Four days after transfection, cells were preincubated for 1 h in resting buffer (5 mM KCl, 120 mM NaCl, 24 mM NaHCO$_3$, 1 mM MgCl$_2$, 2 mM CaCl$_2$, 1 mg/ml ovalbumin, 5 mM HEPES, pH 7.5) and then kept either at rest or in stimulation buffer (25 mM glucose [high glucose {HG}] and 55 mM KCl [high K$^+$ {HK}] in 70 mM NaCl, 24 mM NaHCO$_3$, 1 mM MgCl$_2$, 2 mM CaCl$_2$, 1 mg/ml ovalbumin, and 5 mM HEPES, pH 7.5) for an additional 2 h. In some instances, 30 μM calpeptin or MG-115 (Calbiochem) was added to the stimulation buffer. After 2 h of incubation, cells were washed twice with ice-cold phosphate-buffered saline (PBS) and harvested in ice-cold lysis buffer (20 mM Tris-Cl, pH 8.0, 140 mM NaCl, 1 mM EDTA, 1 mM Triton X-100, and 1% protease inhibitor cocktail [Sigma]). Cell lysates were centrifuged at 4°C and 12,000 rpm for 5 min in an Eppendorf 5415C centrifuge. The precleared soluble protein fraction was separated from the pellet and prepared in SDS-PAGE sample buffer for Western blotting.

Immunoprecipitation (IP). Equal amounts of cell lysates were mixed with 20 μl (1/10 [vol/vol]) protein G-Sepharose beads (GE Healthcare) and incubated on a rotating wheel at 4°C for 30 min to preclear the lysates of the IgG-bound protein fraction. The lysates were centrifuged at 2,000 rpm for 3 min in an Eppendorf centrifuge, and the pellets of beads were removed. Goat anti-GFP antibodies (MPI-CBG, Dresden, Germany) or

IgG from goat serum (Sigma) (1:100 dilution) was then incubated with the precleared lysates overnight prior to the addition of 20 μl (1/10 [vol/vol]) protein G-Sepharose beads. The lysates were centrifuged at 2,000 rpm for 3 min, and the soluble fraction was removed. The beads were washed twice with PBS, centrifuged as described above, and resuspended in SDS-PAGE sample buffer for Western blotting.

Enzymatic deglycosylation assays. INS-1 cells transfected for expression of different ICA512 variants or mouse or human islet cells were incubated in resting or stimulation buffer for 2 h. Cells were lysed as described above and incubated in denaturation buffer (New England BioLabs) at 95°C for 5 min. The denatured samples of the cell lysates were then incubated with peptide-N-glycosidase F (PNGase F), endoglycosidase H or O-glycosidases, endo-α-N-acetylgalactosaminidase, and neuramidase in 1× reaction buffer (New England BioLabs) at 37°C for 3 h. Glycosylated fetuin from fetal calf serum (Sigma) was used as a control to confirm the performance of glycosidases. Nontreated and enzyme-treated cell lysates were prepared in SDS-PAGE sample buffer for Western blotting.

Western blotting. Cell lysates and IPs in SDS-PAGE sample buffer were heated to 95°C for 5 min and then subjected to SDS-PAGE and Western blotting. The following primary antibodies were employed: mouse monoclonal anti-GFP antibody (632381; Clontech), mouse anti-ICA512 antibody HM-1 (23), mouse anti-γ-tubulin antibody (T6557; Sigma), and rabbit anti-HA antibody (ab9110; Abcam). Primary antibodies were detected with horseradish peroxidase (HRP)-conjugated goat anti-mouse or anti-rabbit IgG (Bio-Rad) followed by addition of substrates for chemiluminescence (Thermo Scientific, Pierce Biotechnology), using an LAS-3000 imaging system (Fuji). Black dividing lines in figures indicate cutting of the same or different Western blots or their groupings.

Immunostaining and confocal microscopy. INS-1 cells transfected for the expression of different ICA512 variants and grown on coverslips on 35-mm dishes for 4 days posttransfection were incubated in resting or stimulation buffer as described above, rinsed 3 times in PBS, and fixed with 4% paraformaldehyde. After aldehyde quenching and permeabilization (200 mM glycine, 0.1% Triton X-100 in PBS) for 20 min, cells were incubated in blocking buffer (0.2% gelatin, 0.5% albumin in PBS) for 1 h and then in blocking buffer with guinea pig anti-insulin antibody (ab7842; Abcam) or rabbit anticalnexin antibody (C4731; Sigma) at 4°C overnight. Next, cells were washed 5 times with PBS and then incubated in blocking buffer with Alexa Fluor 568-conjugated goat anti-guinea pig or anti-rabbit IgG (Molecular Probes) for 2 h at room temperature. After additional washing 5 times with PBS, immunolabeled coverslips were mounted onto slides with Mowiol.

INS-1 live-cell staining with the endoplasmic reticulum (ER) tracker red dye (glibenclamide BODIPYTR; Molecular Probes) was done according to the manufacturer's protocol. ICA512 mature ectodomain- or cytosolic domain-specific antibodies (see above), the anti-ME ICA512 antibody, or the anti-ICA512 CT antibody was incubated with living INS-1 cells to assess ICA512 extracellular domain exposure at the cell surface. Images of labeled cells were acquired with an Olympus FluoView-1000 laser scanning confocal microscope equipped with a 60× PlanoApo OLSM lens (numerical aperture [NA] = 1.10).

Cell sorting. Four days after transfection with ICA512-GFP, ICA512-GFP G553D, or ICA512-GFP N506A/N524A, cells were detached by trypsin digestion and resuspended in 1× PBS, 25 mM HEPES (pH 7.0), 1 mM EDTA, and 1% albumin. The cell suspension was filtered through cell strainer caps into 5-ml round-bottom Falcon tubes (Corning) prior to sorting for GFP expression with a Becton Dickinson BD FACS Aria II flow cytometer. Sorted cells expressing the ICA512-GFP variants were cultured in 24-mm culture dishes (Costar) with RPMI 1640 medium.

Insulin gene expression, contents, and secretion. After 2 days in culture, the total RNA of 1×10^5 cells sorted for the expression of each ICA512-GFP variant was purified with a Qiagen RNeasy kit and used as an RNA template for first-strand cDNA synthesis with SuperScript II reverse transcriptase (Invitrogen) and an oligo(dT) primer. Levels of insulin

mRNA were analyzed by quantitative real-time PCR with a GoTaq quantitative PCR kit (Promega) and an MX4000 thermocycler (Stratagene). β-Actin mRNA was amplified in parallel for normalization of the insulin mRNA levels in the individual samples. Alternatively, 3×10^5 ICA512-GFP$^+$ sorted cells were switched to resting buffer for preincubation for 1 h and then to resting or stimulation buffer for an additional 2 h before being harvested for analyses of proinsulin/insulin content and insulin secretion under static conditions by use of a rat/mouse proinsulin/rat insulin enzyme-linked immunosorbent assay (ELISA) (Mercodia).

Statistical analysis. All data are representative of three or more independent experiments, with the exception of the analysis of human islet cells, which was performed two times. Statistical significance was assessed with Student's t test or analysis of variance (ANOVA).

RESULTS

proICA512 dimerizes in INS-1 cells. ME ICA512 encompasses amino acids 449 to 575 of human ICA512 (Fig. 1A). The X-ray structure of recombinant ME ICA512 (Fig. 1B) (18), encompassing amino acids 468 to 558, revealed that this region displays a ferredoxin-like fold related to the SEA (sea urchin sperm protein, enterokinase, agrin) domain, which is known to promote oligodimerization (24–28). Accordingly, both crystallized (18) and soluble (19) versions of ME ICA512 form dimers resulting from the antiparallel pairing of β2-β2 or β4-β4 strands (Fig. 1B) (19).

To verify the occurrence of ICA512 dimers in insulin-producing cells, full-length ICA512 constructs differentially tagged at the C terminus with GFP (ICA512-GFP) or an HA epitope (ICA512-HA) (Fig. 2A) were transiently expressed alone or together in rat insulinoma INS-1 cells. Consistent with previous findings (29, 30), the mature transmembrane fragments (TMF) of ICA512-GFP (ICA512-TMF-GFP; ~100 kDa) and ICA512-HA (ICA512-TMF-HA; ~75 kDa) were the major ICA512 species detected in cell lysates of resting (R) INS-1 cells (Fig. 2A). In cells stimulated (S) with 25 mM glucose, with or without 55 mM KCl, the respective proICA512 species became the most prominent species, while the levels of the corresponding ICA512-TMF, which undergoes calpain-mediated cleavage upon SG exocytosis (29, 30), were drastically reduced. Stimulation with 55 mM KCl alone, which prompts SG exocytosis, also reduced the levels of ICA512-TMF but barely upregulated those of proICA512. The detection of multiple proICA512 species reflects the different degrees of glycosylation of the protein during its maturation along the secretory pathway prior to cleavage and conversion into ICA512-TMF. Notably, in cells stimulated with 55 mM KCl alone, the major proICA512 form migrated faster than the proICA512 species detected in cells concomitantly exposed to high glucose. This discrepancy conceivably reflects differences in the efficiency of proICA512 N-glycosylation in the ER depending on the glucose level.

proICA512-HA and ICA512-TMF-HA were readily detectable, albeit at lower levels when coexpressed with ICA512-GFP (Fig. 2B). Immunoprecipitation with anti-GFP antibodies led to the recovery of ICA512-TMF-GFP or proICA512-GFP from resting or stimulated cells, respectively (Fig. 2C, top panel). Coimmunoprecipitation of proICA512-HA but not ICA512-TMF-HA suggests that proICA512 but not ICA512-TMF forms dimers (Fig. 2C, bottom panel). Neither ICA512-GFP nor ICA512-HA coimmunoprecipitated with control IgGs.

ME ICA512 mediates the dimerization of proICA512 in INS-1 cells. Previous studies *in vitro* and in transfected INS-1 cells indicated that the intracellular PTP domain of ICA512 can dimerize (15, 16). To verify whether ME ICA512 could account for proICA512 dimerization independently of the cytoplasmic domain, INS-1 cells were transfected with ICA512-HA either alone or in combination with soluble ME ICA512-GFP (Fig. 2D, left panel). The slowest electrophoretic species of ME ICA512 was upregulated in stimulated cells and migrated at the expected size of ca. 50 kDa, also taking into account its N-glycosylation. The fastest-migrating species corresponded to the nonglycosylated form of ME ICA512-GFP (also see below and Fig. 5D). Immunoprecipitation of ME ICA512-GFP led to the specific recovery of proICA512-HA from both resting and stimulated cells (Fig. 2D, right panel). Hence, consistent with *in vitro* structural and biochemical analyses (18, 19), ME ICA512 was sufficient to induce the dimerization of proICA512 in INS-1 cells.

Lack of N-glycosylation or perturbation of the β2-β2 association interface of ME ICA512 does not preclude SG sorting and conversion of ICA512. An electrophoretic mobility shift of ICA512 upon digestion with PNGase F indicated that the protein is N-glycosylated (17) (also see below and Fig. 4C and 8D). ICA512 contains only two consensus sites for N-glycosylation, at N506 and N524, both within ME ICA512 (Fig. 1A and B). N506 is located in the β2-strand (Fig. 1B), a critical structural element for β2-β2 dimerization (19). The consensus sequence for N506 glycosylation includes S508, which was shown to mediate β2-β2 dimerization of ME ICA512 *in vitro* (19). N524 is instead remote from the identified dimerization interfaces (Fig. 1B).

To verify the glycosylation of both N506 and N524, INS-1 cells were independently transfected with the single mutants ICA512-GFP N506A, ICA512-GFP S508A, and ICA512-GFP N524A or the double mutant ICA512-GFP N506A/N524A. ICA512-TMF of all ICA512-GFP mutants, as detected with the anti-GFP or anti-ICA512 HM-1 antibody, displayed a faster electrophoretic mobility than that of wild-type ICA512 in resting cells (Fig. 3A). A similar behavior was observed for the corresponding proICA512-GFP species in resting and stimulated cells (Fig. 3A and B). Thus, both N506 and N524 are glycosylated. The expression of proICA512-GFP N506A/N524A was significantly higher than that of ICA512-GFP or single N-glycosylation ICA512-GFP mutants (Fig. 3C), conceivably due to its delayed folding, traffic, and conversion. Lack of N-glycosylation, however, did not prevent the sorting of ICA512-GFP N506A/N524A into SGs, as indicated by its colocalization with insulin at the cell periphery of INS-1 cells, similar to that of ICA512-GFP (Fig. 3D). Notably, ICA512-GFP S508A, for which β2-β2 dimerization should be perturbed (19), was also sorted into SGs (Fig. 3D).

The total level of insulin mRNA in ICA512-GFP N506A/N524A$^+$ sorted cells was not significantly changed compared to that in ICA512-GFP$^+$ sorted cells (Fig. 3E). Likewise, in ICA512-GFP N506A/N524A$^+$ sorted cells, the proinsulin (Fig. 3F) and insulin (Fig. 3G) contents and the fractional stimulated insulin secretion level (Fig. 3H) were not significantly reduced compared to those in ICA512-GFP$^+$ sorted cells.

Perturbation of the ME ICA512 β4-β4 association interface precludes SG sorting and conversion of ICA512. The replacement of G553, which sterically and electrostatically hinders β4-β4 dimerization (19), profoundly altered the maturation and stability of ICA512, in contrast to the case for the replacement of N506 or S508 in the β2-β2 interface. Specifically, the expression of ICA512-TMF-GFP G553D was dramatically reduced (Fig. 4A and B, lanes 4). This was also the case upon cell treatment with the proteasome inhibitor MG-115 (Fig. 4A, lane 6) or calpeptin
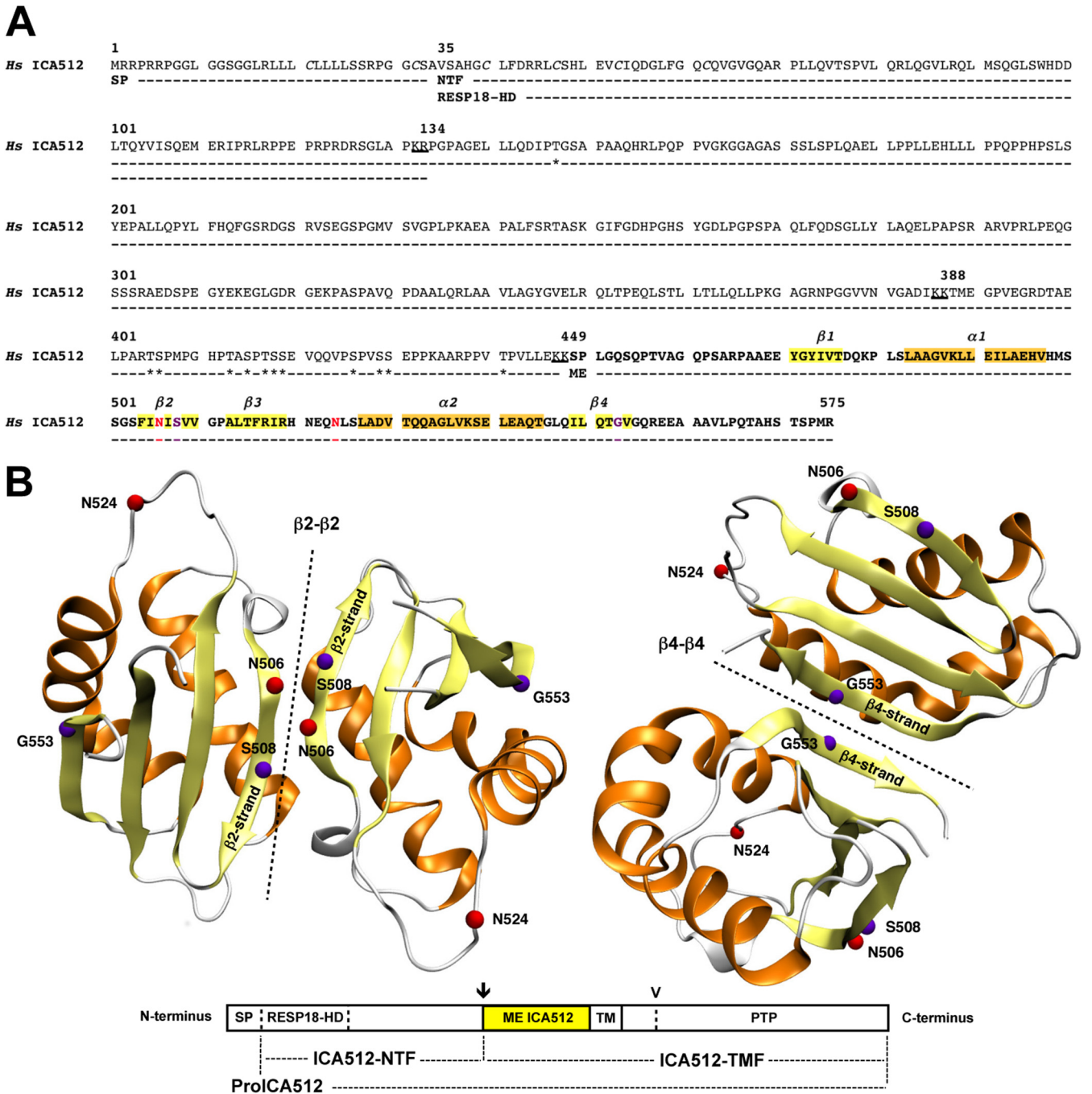
FIG 1 Sequence of the ICA512 extracellular domain and model of ME ICA512 dimerization through β2-β2 and β4-β4 interfaces. (A) Primary amino acid sequence of human (*Hs*) ICA512 extracellular domain (amino acid residues 1 to 575), including the signal peptide (SP) (residues 1 to 34), the RESP18 homology domain (RESP18-HD) (residues 35 to 133), as a part of the N-terminal fragment (NTF) (residues 35 to 448), and the mature ectodomain (ME) (residues 449 to 575 [in bold]). Residues in α-helices and β-strands of ME ICA512, as resolved in reference 18, are highlighted in orange and yellow, respectively. The N-glycosylation sites N506 and N524 are indicated in red, and cleavage sites for protein convertases (KR [residues 132 and 133], KK [residues 386 and 387], and KK [residues 447 and 448]) are underlined. Clustered cysteines within the RESP18-HD (C40, C47, C53, and C62) are indicated in italics, while threonines and serines predicted as putative *O*-glycosylation sites are indicated with asterisks. Critical residues for β2-β2 (S508)- or β4-β4 (G553)-mediated dimerization of recombinant ME ICA512 *in vitro* are shown in purple. (B) Modeled β2-β2 (left) and β4-β4 (right) ME ICA512 dimers (symmetry axes are shown by dotted lines) as resolved by X-ray crystallography (18). The color code for the relevant residues and secondary structures is the same as that described for panel A. The schematic drawing of ICA512 below the models shows the extracellular domain regions described for panel A, followed by the transmembrane (TM) region and the cytosolic PTP domain. The arrow and arrowhead indicate the cleavage site for conversion of proICA512 into ICA512-TMF and the more distal cleavage site for calpain in the cytoplasmic domain of ICA512-TMF, respectively.
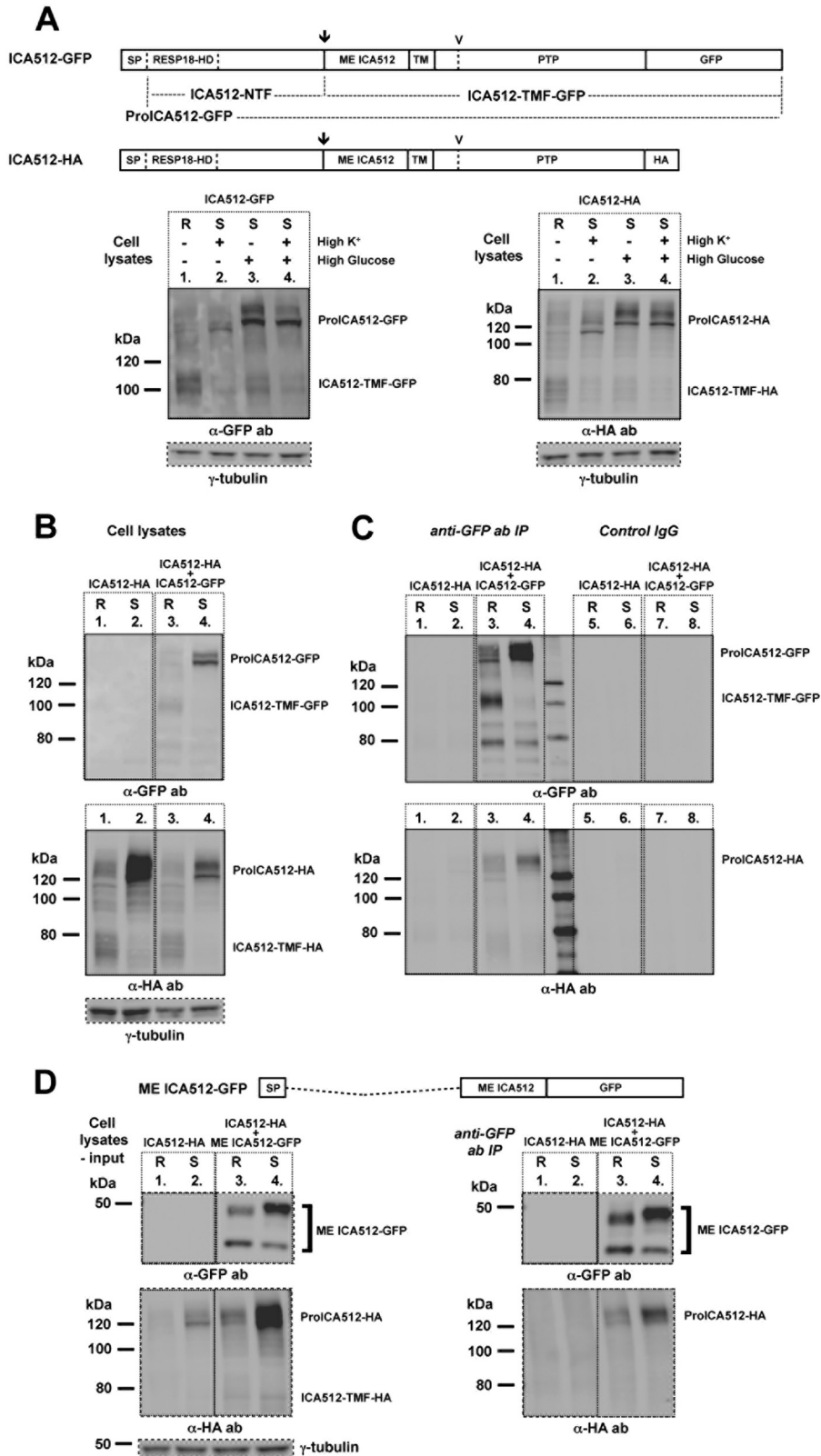
FIG 2 ME ICA512 is sufficient for dimerization of proICA512 in INS-1 cells. (A) Schematic drawings of ICA512-GFP and ICA512-HA and their detection by immunoblotting with mouse anti-GFP or rabbit anti-HA antibody in lysates of singly transfected INS-1 cells. The arrows indicate the cleavage site for conversion of proICA512 into ICA512-TMF, while the arrowheads indicate the more distal calpain cleavage site in the cytoplasmic domain of ICA512-TMF. Prior to lysis, cells were either kept at rest (R) in 0 mM glucose and 5 mM KCl or stimulated (S) for 2 h with either 55 mM KCl (high K$^+$), 25 mM glucose (high glucose), or both (high glucose and high K$^+$ [HGHK]) ($n \geq 3$). (B) Immunoblotting for HA or GFP in lysates of INS-1 cells transfected with ICA512-HA alone or together

(Fig. 4B, lane 6), which prevents the calpain-mediated cleavage of ICA512-TMF, and thus its disappearance (Fig. 4B, lane 3). These observations suggested that the G553D replacement prevents the conversion of proICA512-GFP into ICA512-TMF-GFP. Conversely, expression of ICA512-GFP G553D correlated with the enrichment of proteolytic fragments, mostly in resting cells (Fig. 4A and B, lanes 1 and 4) but also in stimulated cells treated with MG-115 (Fig. 4A, lanes 3 and 6) or calpeptin (Fig. 4B, lanes 3 and 6). Notably, proICA512-GFP G553D appeared as a single band with an electrophoretic mobility comparable to that of the fastest-migrating species of proICA512-GFP (Fig. 4A and B, lanes 2 versus lanes 5). Sensitivity to PNGase F treatment indicated that this phenotype is not attributed to a lack of N-glycosylation (Fig. 4C). Analysis by confocal microscopy further indicated that ICA512-GFP G553D (Fig. 4D, left panels), unlike ICA512-GFP and ICA512-GFP S508A (Fig. 3D), did not colocalize with insulin (Fig. 4D, left panels) but was dispersed throughout the cytoplasm, with a reticular pattern resembling that of the ER tracker red dye (Fig. 4D, right panels). These data suggested that ICA512-GFP G553D is retained within the ER.

In ICA512-GFP G553D$^+$ sorted cells, similar to ICA512-GFP N506A/N524A$^+$ sorted cells (see above and Fig. 3), the total level of insulin mRNA was not changed (Fig. 4E). The proinsulin (Fig. 4F) and insulin (Fig. 4G) contents and the fractional stimulated insulin release level (Fig. 4H) were also not significantly changed relative to those of ICA512-GFP$^+$ sorted cells.

ICA512 is O-glycosylated. ME ICA512 possesses a SEA domain fold, which is present in some mucins and other membrane proteins. SEA domain-containing proteins are commonly extensively O-glycosylated near this domain, possibly to hinder its proteolysis (25, 27, 28). We therefore wondered whether ICA512 is also O-glycosylated and whether this modification, which occurs mainly in the Golgi apparatus, would be affected by the G553D replacement.

O-Glycosidase treatment increased the electrophoretic mobility of the O-glycosylated control protein fetuin (Fig. 5A), as well as that of ICA512-TMF-GFP (Fig. 5B, lane 1 versus lane 2), in extracts of resting cells. De-O-glycosylation of lysates from stimulated cells led to the almost complete disappearance of the slowest-migrating species of proICA512-GFP (Fig. 5B, lane 3 versus lane 4). A comparable mobility shift of ICA512-TMF was observed upon O-glycosidase treatment of lysates of mouse and human islet cells (Fig. 5C), thus indicating that this modification, similar to N-glycosylation (17), also occurs in nontransformed ICA512-expressing tissues. proICA512-GFP N506A (Fig. 5B, lane 5 versus lane 6 and lane 7 versus lane 8) and proICA512-GFP S508A (Fig. 5B, lane 9 versus lane 10 and lane 11 versus lane 12), as well as the corresponding ICA512-TMF forms (Fig. 5B, lane 5 versus lane 6 and lane 9 versus lane 10), were also O-glycosidase sensitive. Conversely, the single proICA512-GFP G553D species was O-glycosidase insensitive (Fig. 5B, lane 15 versus lane 16), consistent with its retention in the ER (Fig. 4D).

**Relevance of the NTF domain for O-glycosylation and export of proICA512 from the ER.** Soluble ME ICA512-GFP, ME ICA512-GFP S508A, and ME ICA512-GFP G553D (Fig. 5D, lanes 1, 5, and 9) were reduced to a single band upon treatment with the N-glycosidase endoglycosidase H (Fig. 5D, lanes 2, 6, and 10) or PNGase F (Fig. 5D, lanes 3, 7, and 11) but were insensitive to O-glycosidases (Fig. 5D, lanes 4, 8, and 12). Thus, multiple ME ICA512-GFP species result from N-glycosylation alone. However, the endoglycosidase H sensitivity of all these ME ICA512 variants further indicated that these retain the high-mannose-structure N-oligosaccharide chains, i.e., they are not exported from the ER. Indeed, confocal microscopy indicated that ME ICA512-GFP or its G553D variant was found to accumulate in the ER (Fig. 5E), concurrent with the lack of O-glycosylation.

Sequence analysis of ICA512 with NetOGlyc 3.1 (31) pointed to serines and threonines clustered within amino acid residues 400 to 440, i.e., in the NTF domain (13, 17), preceding ME ICA512, as the most likely sites for O-glycosylation (Fig. 1A). Nonetheless, the deletion mutant ICA512-GFP ΔNTF, which lacks amino acid residues 35 to 448 (Fig. 1A), i.e., the entire NTF domain, as well as the corresponding ICA512-GFP ΔNTF S508A and ICA512-GFP ΔNTF G553D mutants, was both PNGase F (Fig. 5F, lanes 3, 7, and 11) and O-glycosidase (Fig. 5F, lanes 4, 8, and 12) sensitive. Notably, ICA512-GFP ΔNTF and ICA512-GFP ΔNTF G553D displayed comparably lower electrophoretic mobilities than that of ICA512-GFP ΔNTF S508A, suggesting their similar glycosylations at N506 and N524. Moreover, ICA512-GFP ΔNTF G553D, similar to all other constructs lacking the NTF domain, was endoglycosidase H resistant (Fig. 5F, lanes 2, 6, and 10) and, unlike ICA512-GFP G553D, did not undergo extensive proteolysis. Evidence that proICA512 mutants lacking the NTF domain can fold and exit from the ER even if the ME ICA512 β4-β4 dimerization interface is perturbed suggests that this region contains information for retention of unfolded proICA512 in the ER.

ICA512-NTF is required for targeting of proICA512 to SGs. To further verify the progression of ICA512-GFP ΔNTF along the secretory pathway, we imaged its localization in nonpermeabilized resting (Fig. 6A and B) or stimulated (Fig. 6C) INS-1 cells kept at 4°C to block endocytosis. Both ICA512-GFP and ICA512-GFP ΔNTF, as detected by GFP fluorescence, appeared to be enriched at the cell periphery (Fig. 6A to C). However, labeling with a novel mouse anti-ME ICA512 antibody revealed that ICA512-GFP ΔNTF, unlike ICA512-GFP, was exposed at the cell surface even under resting conditions (Fig. 6A). As expected, the concomitant control labeling of resting cells for insulin, which, like ICA512-GFP, should be confined mainly to SGs and not exposed at the surface, was negative (Fig. 6A). Surface labeling with a mouse anti-ICA512 CT antibody was also negative (Fig. 6B). Conversely, the anti-ME ICA512 antibody labeled the surfaces of both ICA512-GFP- and ICA512-GFP ΔNTF-expressing stimulated cells, albeit more prominently in the case of the latter cells (Fig. 6C). Thus, ICA512-GFP ΔNTF, unlike ICA512-GFP, is constitutively targeted to the cell surface.

Immunoblotting with anti-GFP (Fig. 6D) or anti-ME ICA512 (Fig. 6E) antibody indicated that unlike ICA512-GFP (Fig. 6D and

---

with ICA512-GFP. Prior to lysis, the cells were either kept at rest (R) or stimulated (S) for 2 h with HGHK ($n \geq 3$). For normalization, the same cell lysates were also immunoblotted for γ-tubulin. (C) Immunoblotting for HA or GFP in immunoprecipitates obtained using goat anti-GFP antibody or goat IgG from the lysates shown in panel B ($n \geq 3$). (D) Schematic drawing of ME ICA512-GFP and immunoblotting for HA or GFP in lysates and corresponding immunoprecipitates, obtained using goat anti-GFP antibody, from INS-1 cells transfected with ICA512-HA alone or together with ME ICA512-GFP. Prior to lysis, the cells were kept at rest (R) or stimulated (S) for 2 h with HGHK ($n \geq 3$). For normalization, the same cell lysates were also immunoblotted for γ-tubulin.
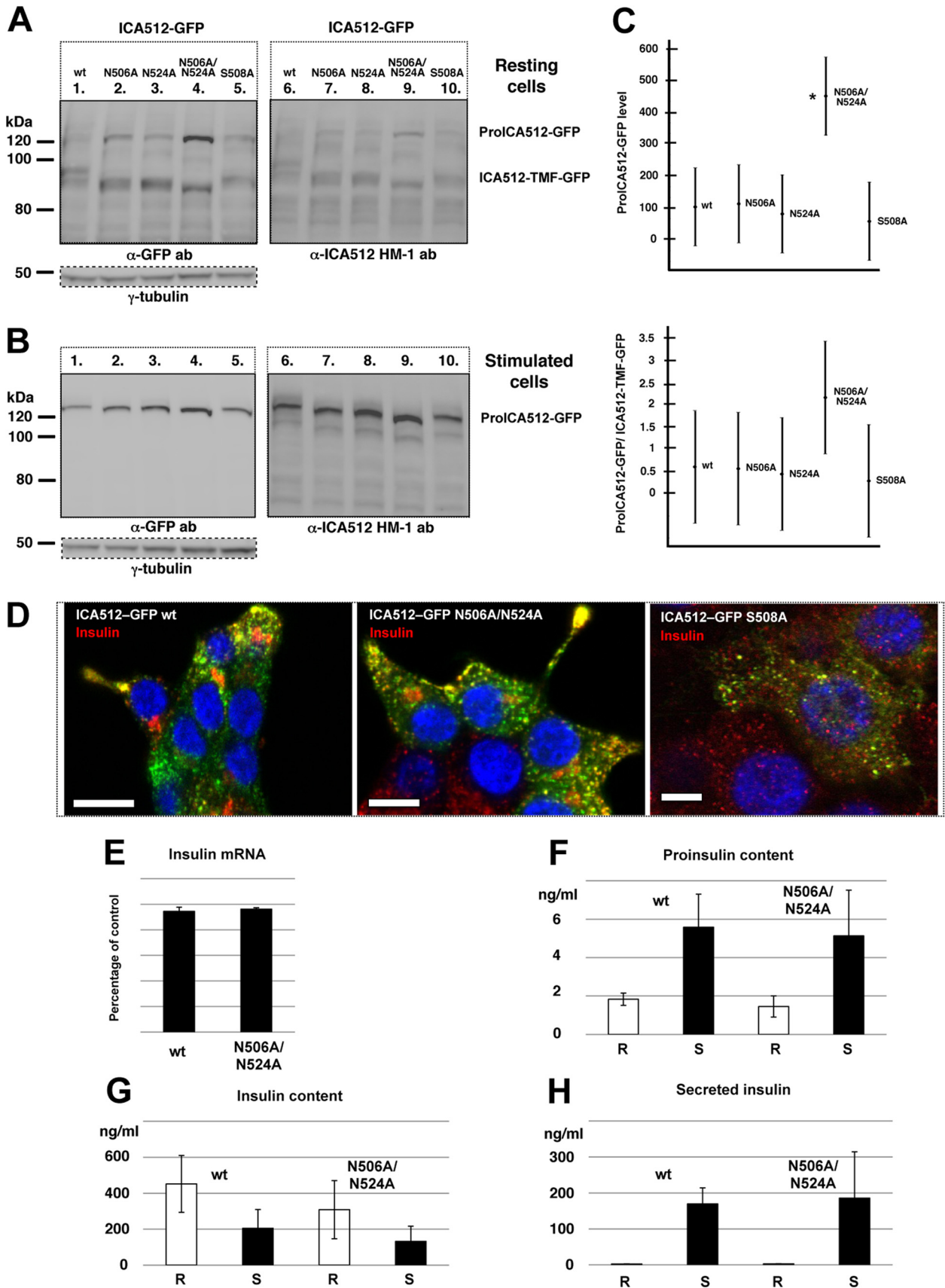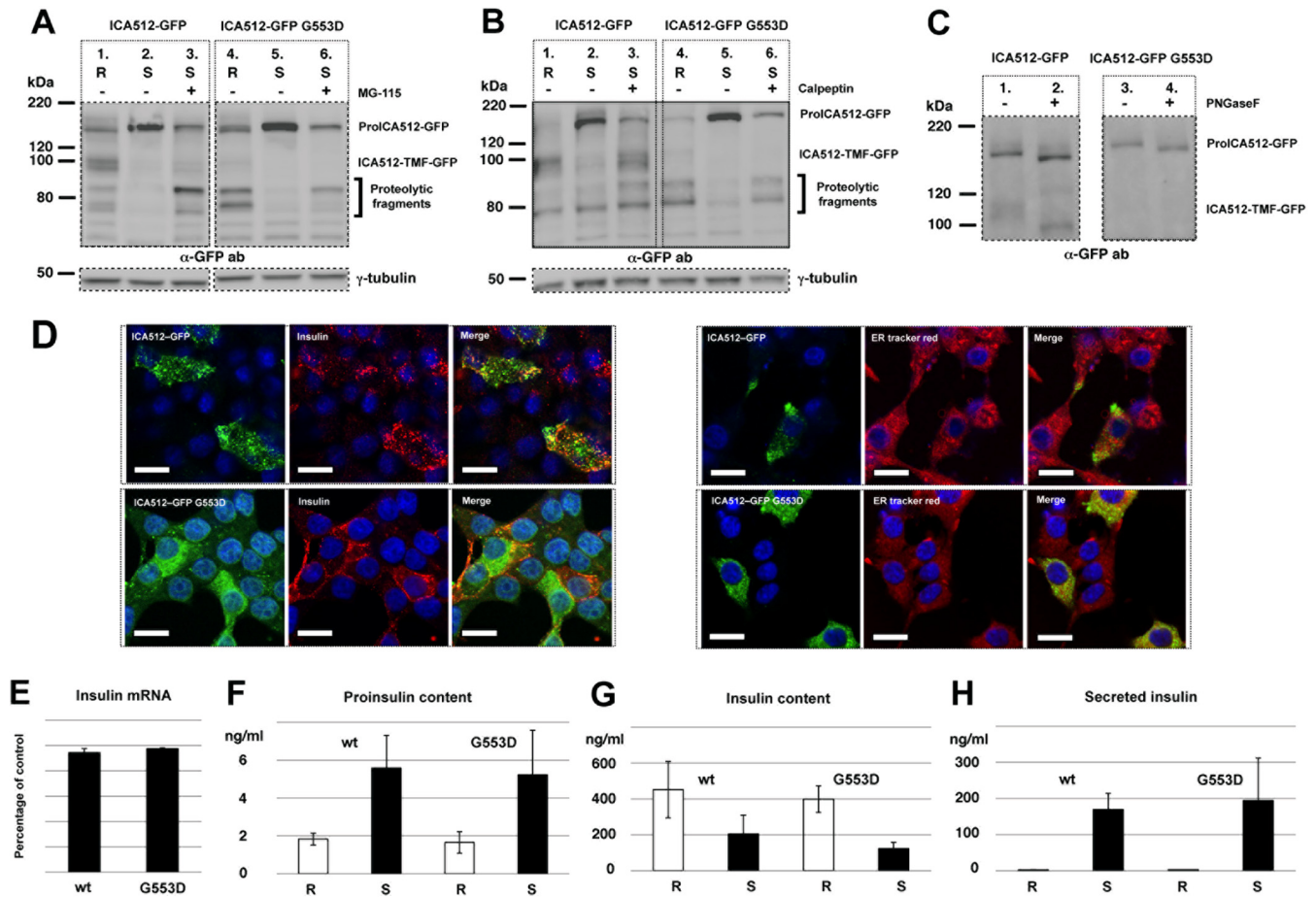
FIG 4 Perturbing the ME ICA512 β4-strand impairs proICA512 stability and targeting to SGs. (A and B) Immunoblotting for GFP in lysates of resting (R) or HGHK-stimulated (S) INS-1 cells transfected with ICA512-GFP or ICA512-GFP G553D and left untreated (−) or treated (+) with the protease inhibitor MG-115 (A) or calpeptin (B) ($n \geq 3$). For normalization, the same cell lysates were also immunoblotted for γ-tubulin. (C) Immunoblotting for GFP in lysates of HGHK-stimulated INS-1 cells transfected with ICA512-GFP or ICA512-GFP G553D and left untreated (−) or treated (+) with the N-glycosidase PNGase F ($n \geq 3$). (D) Confocal microscopy images of HGHK-stimulated INS-1 cells transfected with ICA512-GFP (top panels) or the corresponding G553D mutant (bottom panels) and immunostained for insulin (red; left panels) or colabeled with ER tracker red dye (red; right panels) ($n \geq 3$). Nuclei were labeled with DAPI (in blue). Bars = 5 μm. (E) Insulin mRNA levels ($n = 3$). (F) Proinsulin levels ($n = 3$). (G) Insulin levels ($n = 3$). (H) Secreted insulin levels ($n = 3$).

E, lane 1 versus lane 2), ICA512-GFP ΔNTF (Fig. 6D and E, lane 3 versus lane 4) was not susceptible to Ca^{2+}/calpain-dependent cleavage upon stimulation of INS-1 cells. Hence, the NTF domain is required not only to retain unfolded proICA512 in the ER but also for targeting the latter to SGs, thus enabling the cleavage of ICA512-TMF upon granule exocytosis (29, 30).

The RESP18 homology domain targets proICA512 to SGs. The most N-terminal portion of ICA512-NTF corresponds to the RESP18 homology domain (RESP18-HD) (32), which begins at amino acid residue 35, following the signal peptide, and ends at a

putative cleavage site for protein convertases, between residues 133 and 134 (17) (Fig. 1A). Similar to RESP18 (32, 33), ICA512-RESP18-HD is characterized by a cysteine-rich motif (Fig. 1A), which may be relevant for sorting into SGs. In particular, other characteristic neuroendocrine proteins, such as chromogranin B and secretogranin II, have been shown to depend on disulfide-bonded loops for their targeting to SGs (34–36).

Consistent with the enrichment of RESP18 in SGs (32, 33), soluble ICA512-RESP18-HD-GFP also colocalized extensively with insulin in SG-like structures (Fig. 7A), and its recovery in the

FIG 3 Perturbing N-glycosylation or the ME ICA512 β2-strand does not prevent ICA512 targeting to SGs. (A and B) Immunoblotting for GFP or ICA512 in lysates of resting (A) or stimulated (B) INS-1 cells transfected with either wild-type (wt) ICA512-GFP or the N506A, N524A, N506A/N524A, or S508A mutant ($n \geq 3$). For normalization, the same cell lysates were also immunoblotted for γ-tubulin. (C) Quantification by ANOVA of proICA512-GFP species (top) and of the ratios of the corresponding proICA512-GFP/ICA512-TMF-GFP species (bottom). The mean ± standard error of the mean (SEM) for each ICA512 species was normalized to that for γ-tubulin in the same lysates. *, $P < 0.005$ ($n = 3$). (D) Confocal microscopy images of HGHK-stimulated INS-1 cells transfected with ICA512-GFP wt or the corresponding N506A/N524A or S508A mutant (green) and immunostained for insulin (red) ($n \geq 3$). Nuclei were labeled with DAPI (4′,6-diamidino-2-phenylindole) (blue). Bars = 5 μm. (E) Levels of insulin mRNA in ICA512-GFP wt and ICA512-GFP N506A/N524A sorted cells as measured by reverse transcription-PCR (RT-PCR) and normalized for β-actin mRNA levels ($n = 3$). Levels of proinsulin (F) and insulin (G) in ICA512-GFP wt and ICA512-GFP N506A/N524A sorted cells kept at rest (R) or stimulated (S) for 2 h with HGHK were measured by ELISA ($n = 3$). (H) Insulin secretion measured from ICA512-GFP wt and ICA512-GFP N506A/N524A sorted cells kept at rest (R) or stimulated (S) for 2 h with HGHK ($n = 3$).
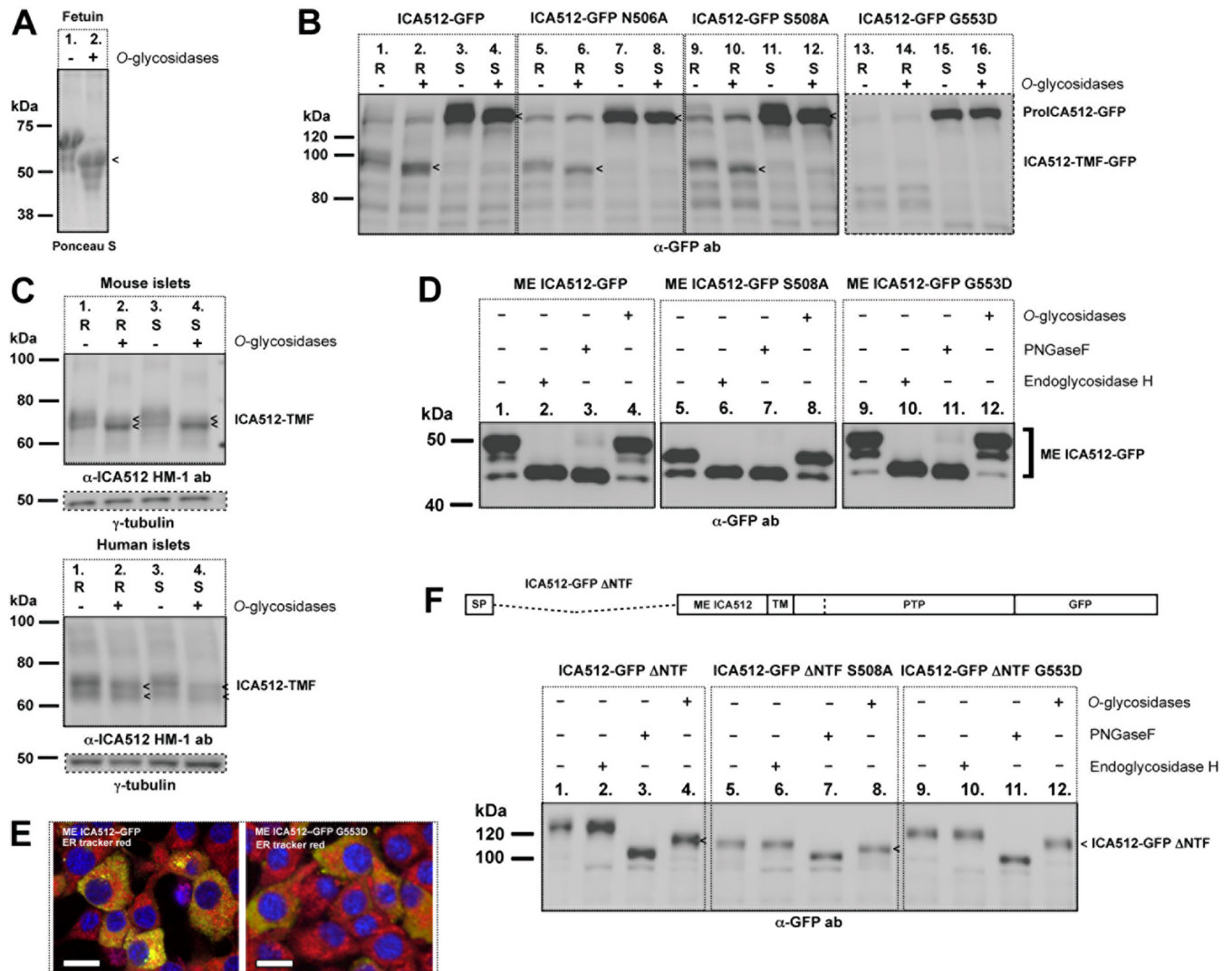
FIG 5 ME ICA512 is *O*-glycosylated. (A) Ponceau S staining of recombinant fetuin left untreated (−) or treated (+) with *O*-glycosidases. (B) Immunoblotting for GFP in lysates of resting (R) or HGHK-stimulated (S) INS-1 cells transfected with ICA512-GFP, ICA512-GFP N506A, ICA512-GFP S508A, or ICA512-GFP G553D and left untreated (−) or treated (+) with *O*-glycosidases (*n* ≥ 3). (C) Immunoblotting for ICA512 in lysates of resting (R) or HGHK-stimulated (S) mouse and human pancreatic islet cells left untreated (−) or treated (+) with *O*-glycosidases (for upper and lower panels, *n* = 3 and *n* = 2, respectively). For normalization, the same lysates were also immunoblotted for γ-tubulin. (D) Immunoblotting for GFP in lysates of HGHK-stimulated INS-1 cells transfected with ME ICA512-GFP, ME ICA512-GFP S508A, or ME ICA512-GFP G553D and left untreated (−) or treated (+) with *O*-glycosidases, PNGase F, or endoglycosidase H (*n* = 3). (E) Merged confocal microscopy images of INS-1 cells transfected with ME ICA512-GFP or ME ICA512-GFP G553D (green) and colabeled with the ER tracker red dye (red) and DAPI (for nuclei; blue) (*n* = 3). Bars = 10 μm. (F) Schematic drawing of ICA512-GFP ΔNTF and immunoblotting for GFP in lysates of HGHK-stimulated INS-1 cells transfected with ICA512-GFP ΔNTF, ICA512-GFP ΔNTF S508A, or ICA512-GFP ΔNTF G553D and left untreated (−) or treated (+) with *O*-glycosidases, PNGase F, or endoglycosidase H (*n* = 3). Fetuin (A) and the ICA512-related protein fragments (B, C, and F) sensitive to *O*-glycosidase treatment (+) are indicated by arrowheads.

medium was enhanced upon stimulation of the cells (Fig. 7B). Conversely, soluble ICA512-NTF-GFP, despite the inclusion of RESP18-HD, displayed a diffuse ER-like pattern (Fig. 7C and D) resembling that of the ER marker calnexin (Fig. 7D). A similar expression pattern was observed for ICA512-NTF (Fig. 7F), as detected with a novel antibody that recognizes human NTF but not the equivalent domain of the endogenous rat protein (Fig. 7E, right panel, lane 1 versus lane 2). These data exclude the possibility that retention of soluble ICA512-NTF in the ER is secondary to its misfolding upon fusion with GFP. Intriguingly, in cells expressing soluble ICA512-NTF-GFP, insulin immunoreactivity was also

more diffuse, rather than being enriched in SGs as in cells expressing ICA512-RESP18-HD-GFP (Fig. 7A). Thus, RESP18-HD contains information that is sufficient for SG targeting, while the remaining portion of ICA512-NTF exerts a dominant role in ER retention, unless it is associated with the remaining C-terminal transmembrane portion of the protein.

The ME ICA512 β4-β4 strand interface is involved in dimerization. Finally, we investigated the occurrence of the main dimerization modes identified in the X-ray structure of nonglycosylated ME ICA512 by using cells (18, 19). The association through a β2-β2 interface was tested by the S508A mutation,
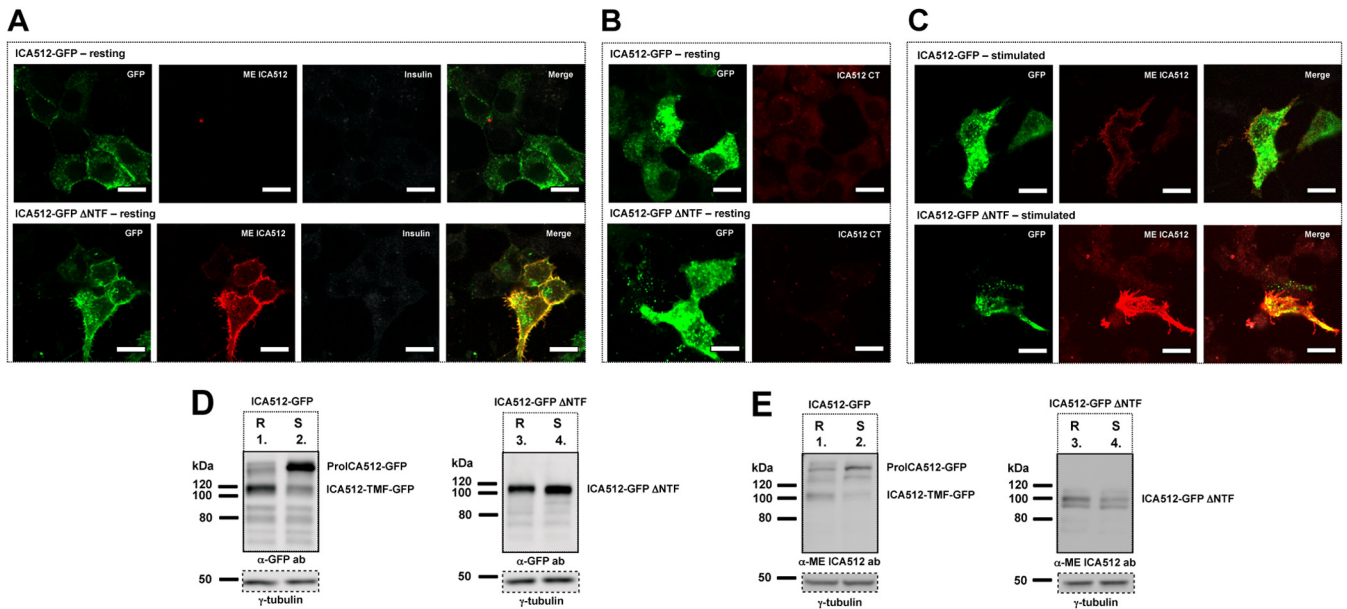
FIG 6 NTF targets ICA512 to SGs. (A to C) Confocal microscopy images of resting (A and B) or HGHK-stimulated (C) INS-1 cells transfected with ICA512-GFP (top panels; green) or ICA512-GFP ΔNTF (bottom panels; green). Live cells were incubated at 4°C with the mouse anti-ME ICA512 antibody (A and C), together with the guinea pig anti-insulin antibody in panel A, or were incubated with the mouse anti-ICA512 CT antibody (B). After fixation, the binding of the primary antibodies to the cell surface was detected by incubation with Alexa Fluor-conjugated anti-mouse (A to C) (red) or anti-guinea pig (A) (white) IgG. Merged images are additionally shown for panels A and C. Bars = 10 μm ($n \geq 3$). (D and E) Immunoblotting for GFP (D) and ME ICA512 (E) in lysates of resting (R) or HGHK-stimulated (S) INS-1 cells transfected with ICA512-GFP or ICA512-GFP ΔNTF ($n \geq 3$). For normalization, the same lysates were also immunoblotted for γ-tubulin.

which impeded dimerization of recombinant nonglycosylated ME ICA512 in vitro (albeit not in the crystal). The second dimerization mode, through the β4-β4 interface, was tested by the G553D replacement, which is sterically incompatible with this mode (19). ICA512-HA and ME ICA512-GFP variants with the symmetric single or combined mutations were coexpressed in INS-1 cells, and the lysates of the stimulated cells and the corresponding immunoprecipitates were analyzed by immunoblotting (Fig. 8A and B). While symmetric replacement of S508 did not preclude the recovery of proICA512-HA S508A with ME ICA512-GFP S508A (Fig. 8B, lane 9), the symmetric replacement of G553 prevented the coimmunoprecipitation of proICA512-HA G553D with ME ICA512-GFP G553D (Fig. 8B, lane 10). The recovery of proICA512-HA mutants with the corresponding ME ICA512-GFP variants was specific, as coimmunoprecipitations with control IgG were significantly less effective than those with the anti-GFP antibody (Fig. 8B, lanes 13 to 18, and C). These findings suggest that dimerization of proICA512 occurs through β4-β4 interactions. Remarkably, however, the combined S508A/G553D replacement was still permissive for ME ICA512 dimerization, although the recovered proICA512-HA S508A/G553D variant displayed a faster electrophoretic mobility (Fig. 8B, lane 11), consistent with a lack of N506 glycosylation. Hence, even upon perturbation of the β4-β4 interface, dimerization may still occur via the β2-β2 interaction, but only under conditions which prevent/precede N506 glycosylation. Glycosylation, because of its bulkiness, would impede the physical contact between β2-strands. Consistent with this interpretation was the greater yield of coimmunoprecipitated proICA512-HA upon replacement of N506 rather than S508 in combination with G553 (Fig. 8B, lane 12, and C).

According to the structural data, N506 is less critical than S508 for the establishment/retention of a β2-β2 dimer interface (19), and thus for protein folding and stability, as corroborated by the

larger amount of proICA512-HA N506A/G553D than of proICA512-HA S508A/G553D in the cell lysate (Fig. 8A, lane 6 versus lane 5). Notably, β2-β2 proICA512 dimers are retained mainly in the ER, as shown in the specific case of proICA512-HA S508A/G553D, which for the most part remained endoglycosidase H sensitive (Fig. 8D, lower panel) and was not converted to the corresponding mature ICA512-TMF species (Fig. 8D, upper panel). Hence, preclusion of N506 glycosylation does not rescue the replacement of G553, but it allows the detection of β2-β2 interface-mediated dimerization of ME ICA512, which under normal conditions may represent only a transient state of the receptor. Once N506 glycosylation occurs, folding of the β4-β4 interface would become critical for stabilization/dimerization of proICA512 and for overcoming the dominant ER retention signal within ICA512-NTF, thus enabling further progression of the protein along the secretory pathway and its RESP18-HD-mediated targeting to the SGs (Fig. 8E).

DISCUSSION

Dimerization of RPTPs has generally been found to occur at the cell surface. This process is driven by the interaction of ligands with the extracellular domain and can affect the phosphatase activity of the cytoplasmic PTP domain. In the case of ICA512, however, no extracellular ligands have yet been identified. Its signaling pathway also remains unclear, although the calpain-cleaved cytosolic fragment generated upon granule exocytosis has been suggested to act as a retrograde signal to modulate insulin SG mobility and biogenesis in relationship to the size and consumption of the SG stores (16, 23, 30). In this work, we have begun to unravel some of the functional properties of the ICA512 SG luminal/extracellular region.

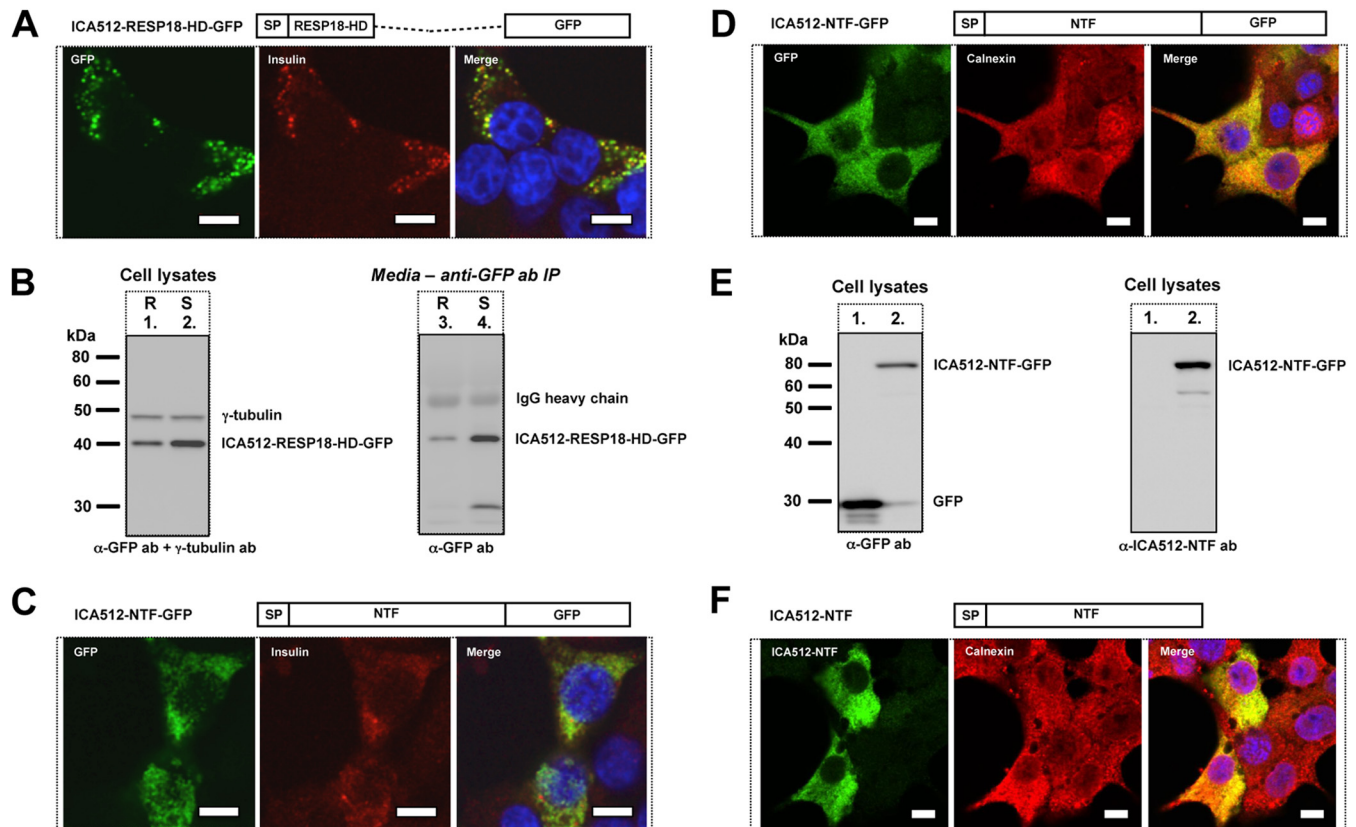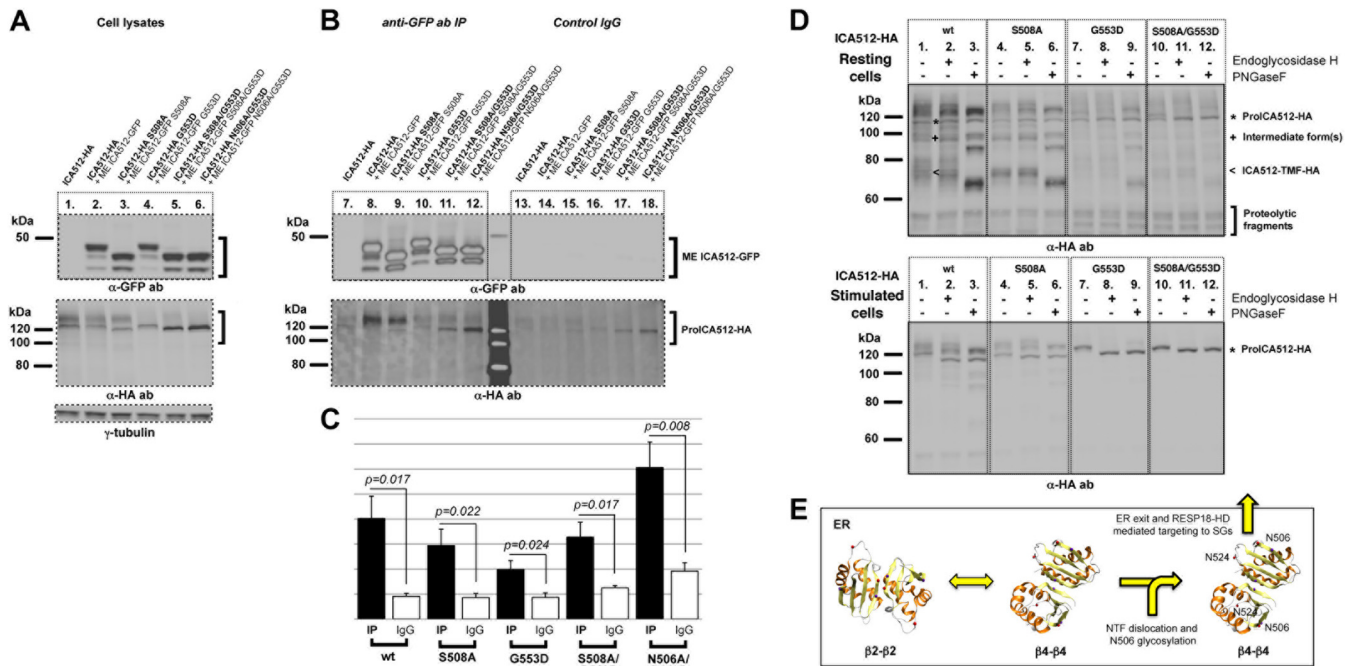Specifically, we showed that ME ICA512 is sufficient to pro-

FIG 7 NTF contains information for both ER retention and SG targeting. (A) Schematic drawing of ICA512-RESP18-HD-GFP and confocal microscopy images of resting INS-1 cells transfected with ICA512-RESP18-HD-GFP (green) and immunostained for insulin (red) ($n \geq 3$). Nuclei were labeled with DAPI (blue). Bars = 5 μm. (B) Immunoblotting for GFP in lysates (left) or immunoprecipitates, obtained with a different, goat anti-GFP antibody from the incubation media (right), of resting (R) and HGHK-stimulated (S) INS-1 cells transfected with ICA512-RESP18-HD-GFP ($n \geq 3$). The cell lysates were also immunoblotted for γ-tubulin. (C and D) Schematic drawings of ICA512-NTF-GFP and confocal microscopy images of resting INS-1 cells transfected with ICA512-NTF-GFP (green) and immunostained for insulin (C) (red) or calnexin (D) (red) ($n \geq 3$). Nuclei were labeled with DAPI (blue). Bars = 5 μm. (E) Immunoblotting for GFP (left) or NTF (right) in lysates of INS-1 cells transfected with either CD33-GFP or ICA512-NTF-GFP (lanes 1 versus lanes 2) ($n \geq 3$). (F) Schematic drawing of ICA512-NTF and confocal microscopy images of INS-1 cells transfected with ICA512-NTF and immunostained for NTF (green) and calnexin (red) ($n \geq 3$). Bars = 5 μm.

mote ICA512 dimerization in cells (Fig. 2D), as suggested by previous structural studies of the corresponding recombinant portion of the receptor (18, 19). Notably, we detected dimers only of proICA512, not ICA512-TMF (Fig. 2C and D), implying that maturation of the protein resolves this interaction such that, in the SGs, ICA512-TMF is present as a monomer. On the other hand, we cannot exclude the possibility that in the granule lumen, ICA512-TMF instead forms a heterodimer with soluble ICA512-NTF generated from convertase-mediated cleavage of proICA512 between residues 448 and 449 (Fig. 1A). Repeated attempts to coimmunoprecipitate ICA512-NTF with ICA512-TMF, however, have been unsuccessful. Since ICA512-NTF contains two additional likely sites for convertase cleavage, between residues 133 and 134 and residues 387 and 388 (Fig. 1A), it is also possible that two putative fragments resulting from these cleavages, of ~28 kDa and ~7 kDa, were not detected by SDS-PAGE and Coomassie blue/silver staining, either being masked by the IgG light chain or due to their small size. Other factors that may disrupt ME ICA512 dimers include posttranslational modifications occurring while the protein transits from the ER to the SGs, the progressive intraluminal acidification of the Golgi and SG compartments, and/or binding to other secretory proteins. Intriguingly, it has

been reported that phogrin/IA-2β interacts with carboxypeptidase E/H (37). Finally, we cannot rule out that ME ICA512 again prompts homodimerization of ICA512-TMF once the latter is transiently inserted into the plasma membrane upon granule exocytosis.

Our data suggest that dimerization of proICA512 occurs in the ER. Supporting this conclusion is the fact that proICA512-GFP G553D accumulates in the ER (Fig. 4D) and does not undergo O-glycosylation (Fig. 5B), a posttranslational modification that most commonly occurs in the Golgi apparatus. However, ICA512-GFP ΔNTF G553D is endoglycosidase H resistant and O-glycosylated (Fig. 5F). These findings, together with evidence that soluble NTF accumulates instead in the ER (Fig. 7C, D, and F), suggest that NTF contains an ER retention signal. In contrast, soluble RESP18-HD-GFP, similar to its paralogue RESP18 (32, 33, 38), is targeted to the SGs (Fig. 7A) and released in a regulated fashion from the cells (Fig. 7B). Accordingly, ICA512-GFP ΔNTF is neither retained in the ER nor targeted to SGs but is constitutively delivered to the cell surface (Fig. 6A to C). Intriguingly, in cells overexpressing soluble NTF but not soluble RESP18-HD, insulin immunoreactivity is also more diffuse and less granular (Fig. 7C). Additional studies on the structures of ICA512-NTF

FIG 8 Establishment of ME ICA512 β4-β4 dimers overcomes the NTF ER retention signal. (A) Immunoblotting for GFP (top) or HA (middle) in the lysates of HGHK-stimulated INS-1 cells transfected with ICA512-HA alone (lane 1) or doubly transfected with ICA512-HA and ME ICA512-GFP (lane 2) or with the respective ICA512-HA and ME ICA512-GFP S508A, G553D, S508A/G553D, or N506A/G553D mutants (lanes 3 to 6). For normalization, the same lysates were also immunoblotted for γ-tubulin (lanes 1 to 6; bottom) ($n \geq 3$). (B) Immunoblotting for GFP (top) or HA (bottom) in immunoprecipitates obtained with a goat anti-GFP antibody (lanes 7 to 12) or control IgG (lanes 13 to 18) from the corresponding cell lysates ($n \geq 3$). (C) Quantification of the immunoprecipitates in panel B. For all comparisons, $n = 5$ and $P < 0.05$. (D) Immunoblotting for HA in endoglycosidase H- or PNGase F-untreated (−) or -treated (+) lysates from resting (top) or HGHK-stimulated (bottom) INS-1 cells transfected with ICA512-HA, ICA512-HA S508A, ICA512-HA G553D, or ICA512-HA S508A/G553D ($n \geq 3$). (E) Model for how N506 glycosylation affects the folding and dimerization of ME ICA512 β2-β2 and β4-β4 association interfaces and the export of proICA512 from the ER.

and RESP18-HD and their roles in SG biogenesis will be necessary to elucidate the reasons for these phenomena.

Extending previous findings (17, 39, 40), we showed that N506 and N524 of ICA512 are both glycosylated (Fig. 3A and B). Lack of glycosylation at these sites does not prevent targeting of proICA512 to SGs (Fig. 3D) and its conversion to ICA512-TMF (Fig. 3A). Simultaneous inhibition of N506 glycosylation and perturbation of the ME ICA512 β2-β2 association interface by replacement of S508A are also insufficient to prevent proICA512 conversion to ICA512-TMF (Fig. 3A) and ME ICA512-mediated homodimerization (Fig. 8B). Conversely, perturbation of the ME ICA512 β4-strand by G553D replacement hinders the stability, SG targeting, and conversion of proICA512 (Fig. 4A to D), as well as its recovery as a homodimer (Fig. 8B). On the other hand, combined S508A/G553D or N506A/G553D replacements are still compatible with proICA512 dimerization (Fig. 8B). A possible explanation for the latter finding is that the extended β2-β2 association interface (19) (Fig. 1A and B) is sufficient for stable proICA512 dimerization provided that glycosylation of N506, as upon S508A replacement, is precluded. This conclusion is corroborated by the greater yield of proICA512 homodimers recovered when the G553D mutation is combined with the N506A replacement, which structural studies predict to be less detrimental than S508A replacement to ME ICA512 β2-β2 interface-mediated dimerization (Fig. 8B and C). Notably, such β2-β2 interface-mediated proICA512 dimers are restricted to the ER, as indicated by

the endoglycosidase H sensitivity and lack of conversion of proICA512-GFP S508A/G553D (Fig. 8D).

In conclusion, we propose a model whereby proICA512 β2-β2 dimers prevail over β4-β4 dimers in the ER as long as the β2-strand N506 is not glycosylated, possibly due to occlusion of this region by NTF. Dislocation of NTF, as upon its binding to another molecule, would allow for N506 glycosylation, thus irreversibly shifting the equilibrium toward proICA512 β4-β4 dimers, consequently allowing ICA512 to leave the ER (Fig. 8E). Importantly, this model does not assume that β4-β4 dimerization *per se* is the signal for ER export. Indeed, ICA512-GFP ΔNTF G553D, in which concomitant glycosylation of N506 and G553D replacement should hinder the formation of both ME ICA512 β2-β2 and β4-β4 dimers, is nevertheless exported from the ER, conceivably as a monomer. Hence, it is plausible that folding and/or homodimerization of ME ICA512 β4-strands are instrumental for stabilizing proICA512 and overcoming the NTF ER retention signal.

REFERENCES

1. **Blanchetot C, Tertoolen LG, Overvoorde J, den Hertog J.** 2002. Intra- and intermolecular interactions between intracellular domains of receptor protein-tyrosine phosphatases. J Biol Chem **277**:47263–47269. http://dx.doi.org/10.1074/jbc.M205810200.

2. **Chin C, Sachs JN, Engelman DM.** 2005. Transmembrane homodimerization of receptor-like protein tyrosine phosphatases. FEBS Lett **579**:3855–3858. http://dx.doi.org/10.1016/j.febslet.2005.05.071.

3. **Tonks NK.** 2006. Protein tyrosine phosphatases: from genes, to function, to disease. Nat Rev Mol Cell Biol **7**:833–846. http://dx.doi.org/10.1038/nrm2039.

4. **Barr AJ, Ugochukwu E, Lee WH, King ON, Filippakopoulos P, Alfano I, Savitsky P, Burgess-Brown NA, Muller S, Knapp S.** 2009. Large-scale structural analysis of the classical human protein tyrosine phosphatome. Cell **136**:352–363. http://dx.doi.org/10.1016/j.cell.2008.11.038.

5. **Mohebiany AN, Nikolaienko RM, Bouyian S, Harroch S.** 2013. Receptor-type tyrosine phosphatase ligands: looking for the needle in the haystack. FEBS J **280**:388–400. http://dx.doi.org/10.1111/j.1742-4658.2012.08653.x.

6. **Abbott KL, Matthews RT, Pierce M.** 2008. Receptor tyrosine phosphatase β (RPTPβ) activity and signaling are attenuated by glycosylation and subsequent cell surface galectin-1 binding. J Biol Chem **283**:33026–33035. http://dx.doi.org/10.1074/jbc.M803646200.

7. **Earl L, Bi S, Baum L.** 2010. N- and O-glycans modulate galectin-1 binding, CD45 signaling, and T cell death. J Biol Chem **285**:2232–2244. http://dx.doi.org/10.1074/jbc.M109.066191.

8. **Zondag GCM, Koningstein GM, Jiang Y, Sap Y, Moolenaar WH, Gebbink MFBG.** 1995. Homophilic interactions mediated by receptor tyrosine phosphatases μ and κ. J Biol Chem **270**:14247–14250. http://dx.doi.org/10.1074/jbc.270.24.14247.

9. **Jiang G, den Hertog J, Hunter T.** 2000. Receptor-like protein tyrosine phosphatase alpha homodimerizes on the cell surface. Mol Cell Biol **20**:5917–5929. http://dx.doi.org/10.1128/MCB.20.16.5917-5929.2000.

10. **Aricescu AR, Hon W, Siebold C, Lu W, van der Merwe PA.** 2006. Molecular analysis of receptor protein tyrosine phosphatase μ-mediated cell adhesion. EMBO J **25**:701–712. http://dx.doi.org/10.1038/sj.emboj.7600974.

11. **Magistrelli G, Toma S, Isacchi A.** 1996. Substitution of two variant residues in the protein tyrosine phosphatase-like PTP35/IA-2 sequence reconstitutes catalytic activity. Biochem Biophys Res Commun **227**:581–588. http://dx.doi.org/10.1006/bbrc.1996.1549.

12. **Torii S.** 2009. Expression and function of IA-2 family proteins, unique neuroendocrine-specific protein-tyrosine phosphatases. Endocr J **56**:639–648. http://dx.doi.org/10.1507/endocrj.K09E-157.

13. **Solimena M, Dirkx R, Jr, Hermel JM, Pleasic-Williams S, Shapiro JA, Caron L, Rabin DU.** 1996. ICA 512, an autoantigen of type I diabetes, is an intrinsic membrane protein of neurosecretory granules. EMBO J **15**:2102–2114.

14. **Wasmeier C, Hutton JC.** 1996. Molecular cloning of phogrin, a protein-tyrosine phosphatase homologue localized to insulin secretory granule membranes. J Biol Chem **271**:18161–18170. http://dx.doi.org/10.1074/jbc.271.30.18161.

15. **Gross S, Blanchetot C, Schepens J, Albet S, Lammers R, den Hertog J, Hendriks W.** 2002. Multimerization of the protein-tyrosine phosphatase (PTP)-like insulin dependent diabetes mellitus autoantigens IA-2 and IA-2β with receptor PTPs (RPTPs). J Biol Chem **277**:48139–48145. http://dx.doi.org/10.1074/jbc.M208228200.

16. **Trajkovski M, Mziaut H, Schubert S, Kalaidzidis Y, Altkrüger A, Solimena M.** 2008. Regulation of insulin granule turnover in pancreatic

17. **Hermel JM, Dirkx R, Jr, Solimena M.** 1999. Post-translational modifications of ICA512, a receptor tyrosine phosphatase-like protein of secretory granules. Eur J Neurosci **11**:2609–2620. http://dx.doi.org/10.1046/j.1460-9568.1999.00677.x.

18. **Primo ME, Klinke S, Sica MP, Goldbaum FA, Jakoncic J, Poskus E, Ermácora MR.** 2008. Structure of the mature ectodomain of the human receptor-type protein-tyrosine phosphatase IA-2. J Biol Chem **283**:4674–4681. http://dx.doi.org/10.1074/jbc.M708144200.

19. **Primo ME, Jakoncic J, Noguera ME, Risso VA, Sosa L, Sica MP, Solimena M, Poskus E, Ermácora MR.** 2011. Protein-protein interactions in crystals of the human receptor-type protein tyrosine phosphatase ICA512 ectodomain. PLoS One **6**:e24191. http://dx.doi.org/10.1371/journal.pone.0024191.

20. **Noguera ME, Primo ME, Sosa LN, Risso VA, Poskus E, Ermácora MR.** 2013. Biophysical characterization of the membrane-proximal ectodomain of the receptor-type protein-tyrosine phosphatase phogrin. Protein Pept Lett **20**:1009–1017. http://dx.doi.org/10.2174/0929866511320090007.

21. **Noguera ME, Primo ME, Jakoncic J, Poskus E, Solimena M, Ermácora MR.** 26 November 2014. X-ray structure of the mature ectodomain of phogrin. J Struct Funct Genomics http://dx.doi.org/10.1007/s10969-014-9191-0.

22. **Asfari M, Janjic D, Meda P, Li G, Halban PA, Wollheim CB.** 1992. Establishment of 2-mercaptoethanol-dependent differentiated insulin-secreting cell lines. Endocrinology **130**:167–178. http://dx.doi.org/10.1210/endo.130.1.1370150.

23. **Mziaut H, Trajkovski M, Kersting S, Ehninger A, Altkrüger A, Lemaitre RP, Schmidt D, Saeger H, Lee M, Drechsel DN, Müller S, Solimena M.** 2006. Synergy of glucose and growth hormone signalling in islet cells through ICA512 and STAT5. Nat Cell Biol **8**:435–445. http://dx.doi.org/10.1038/ncb1395.

24. **Ligtenberg MJ, Kruijshaar L, Buijs F, van Meijer M, Litvinov SV, Hilkens J.** 1992. Cell-associated episialin is a complex containing two proteins derived from a common precursor. J Biol Chem **267**:6171–6177.

25. **Bork P, Patthy L.** 1995. The SEA module: a new extracellular domain associated with O-glycosylation. Protein Sci **4**:1421–1425. http://dx.doi.org/10.1002/pro.5560040716.

26. **Wreschner DH, McGuckin MA, Williams SJ, Baruch A, Yoeli M, Ziv R, Okun L, Zaretsky J, Smorodinsky N, Keydar I, Neophytou P, Stacey M, Lin H, Gordon S.** 2002. Generation of ligand-receptor alliances by "SEA" module-mediated cleavage of membrane-associated mucin proteins. Protein Sci **11**:698–706. http://dx.doi.org/10.1110/ps.16502.

27. **Khatri IA, Wang R, Forstner JF.** 2003. SEA (sea-urchin sperm protein, enterokinase and agrin)-module cleavage, association of fragments and membrane targeting of rat intestinal mucin Muc3. Biochem J **372**:263–270. http://dx.doi.org/10.1042/BJ20021333.

28. **Jonckheere N, Skrypek N, Frénois F, Van Seuningen I.** 2013. Membrane-bound mucin modular domains: from structure to function. Biochimie **95**:1077–1086. http://dx.doi.org/10.1016/j.biochi.2012.11.005.

29. **Ort T, Voronov S, Guo J, Zawalich K, Froehner SC, Zawalich W, Solimena M.** 2001. Dephosphorylation of β2-syntrophin and Ca²⁺/μ-calpain-mediated cleavage of ICA512 upon stimulation of insulin secretion. EMBO J **20**:4013–4023. http://dx.doi.org/10.1093/emboj/20.15.4013.

30. **Trajkovski M, Mziaut H, Altkrüger A, Ouwendijk J, Knoch K, Müller S, Solimena M.** 2004. Nuclear translocation of an ICA512 cytosolic fragment couples granule exocytosis and insulin expression in β-cells. J Cell Biol **167**:1063–1074. http://dx.doi.org/10.1083/jcb.200408172.

31. **Julenius K, Molgaard A, Gupta R, Brunak S.** 2005. Prediction, conservation analysis, and structural characterization of mammalian mucin-type O-glycosylation sites. Glycobiology **15**:153–164. http://dx.doi.org/10.1093/glycob/cwh151.

32. **Bloomquist BT, Darlington DN, Mains RE, Eipper BA.** 1994. RESP18, a novel endocrine secretory protein transcript, and four other transcripts are regulated in parallel with pro-opiomelanocortin in melanotropes. J Biol Chem **269**:9113–9122.

33. **Zhang G, Hirai H, Cai T, Miura J, Yu P, Huang H, Schiller MR, Swaim WD, Leapman RD, Notkins AL.** 2007. RESP18, a homolog of the luminal domain of IA-2, is found in dense core vesicles in pancreatic islet cells and is induced by high glucose. J Endocrinol **195**:313–321. http://dx.doi.org/10.1677/JOE-07-0252.

34. **Gerdes H, Rosa P, Phillips E, Bauerle PA, Frank R, Argos P, Huttner WB.** 1989. The primary structure of human secretogranin II, a widespread

β-cells by cleaved ICA512. J Biol Chem **283**:33719–33729. http://dx.doi.org/10.1074/jbc.M804928200.

tyrosine-sulfated secretory granule protein that exhibits low pH- and calcium-induced aggregation. J Biol Chem **264:**12009–12015.

35. **Thiele C, Gerdes H, Huttner WB.** 1997. Protein secretion: puzzling receptors. Curr Biol **7:**496–500.

36. **Glombik MM, Krömer A, Salm T, Huttner WB, Gerdes H.** 1999. The disulfide-bonded loop of chromogranin B mediates membrane binding and directs sorting from the trans-Golgi network to secretory granules. EMBO J **18:**1059–1070. http://dx.doi.org/10.1093/emboj/18.4.1059.

37. **Saito N, Takeuchi T, Kawano A, Hosaka M, Hou N, Torii S.** 2011. Luminal interaction of phogrin with carboxypeptidase E for effective targeting to secretory granules. Traffic **12:**499–506. http://dx.doi.org/10.1111/j.1600-0854.2011.01159.x.

38. **Schiller MR, Mains RE, Eipper BA.** 1995. A neuroendocrine-specific protein localized to the endoplasmic reticulum by distal degradation. J Biol Chem **270:**26129–26138. http://dx.doi.org/10.1074/jbc.270.44.26129.

39. **Payton MA, Hawkes CJ, Christie MR.** 1995. Relationship of the 37,000- and 40,000-M_r tryptic fragments of islet antigens in insulin-dependent diabetes to the protein tyrosine phosphatase-like molecule IA-2 (ICA512). J Clin Invest **96:**1506–1511. http://dx.doi.org/10.1172/JCI118188.

40. **Notkins AL, Lu J, Li Q, VanderVegt FP, Wasserfall C, Maclaren NK, Lan MS.** 1996. IA-2 and IA-2β are major autoantigens in IDDM and the precursors of the 40 kDa and 37 kDa tryptic fragments. J Autoimmun **9:**677–682. http://dx.doi.org/10.1006/jaut.1996.0088.